Electrical transport properties of TiCoSb half-Heusler phases that exhibit high resistivity

2001 J. Phys.: Condens. Matter 13 77

(http://iopscience.iop.org/0953-8984/13/1/308)

INSTITUTE OF PHYSICS PUBLISHING JOURNAL OF PHYSICS: CONDENSED MATTER

J. Phys.: Condens. Matter **13** (2001) 77–89 www.iop.org/Journals/cm PII: S0953-8984(01)13497-1

Electrical transport properties of TiCoSb half-Heusler phases that exhibit high resistivity

Y Xia[1], V Ponnambalam[1], S Bhattacharya[2], A L Pope[2], S J Poon[1] and T M Tritt[2]

[1] Department of Physics, University of Virginia, Charlottesville, VA 22901, USA
[2] Department of Physics and Astronomy, Clemson University, Clemson, SC 29634, USA

Received 25 April 2000, in final form 19 October 2000

Abstract

Electrical transport measurements have been performed on doped and undoped TiCoSb half-Heusler phases. The semiconducting properties are found to be more robust than those reported for MNiSn (M = Ti, Zr, Hf). Undoped TiCoSb phases exhibit large n-type Seebeck coefficients and high resistivities that reach -500 μV K^{-1} at 300 K and $\sim$1500 Ω cm at 4.2 K, respectively. A tendency towards carrier localization is seen in several disordered phases. The effects due to n-type and p-type dopants are readily manifested in the thermopower, from which moderately heavy electron and hole band masses are inferred. The unusual properties measured are consistent with the prediction of a wide bandgap for the TiCoSb phase. A resistivity minimum is observed at 500–600 K for undoped and V-doped TiCoSb. Consequently, the semiconducting gap has not been determined.

1. Introduction

A class of semiconducting intermetallic compounds of formula MNiSn (M = Ti, Zr, Hf) was discovered a decade ago [1, 2]. These compounds crystallize in the MgAgAs-type structure [3] and are known as the half-Heusler phases. The crystal structure is built from three interpenetrating face-centred cubic (fcc) sublattices of equal unit-cell size. Two of the fcc sublattices combine to form a rock-salt substructure (MSn in the case of MNiSn) and the third fcc sublattice is displaced along the body diagonal of the rock-salt substructure by one quarter of the unit cell. The MNiSn phases were found to exhibit n-type electronic transport properties that included a large thermopower Seebeck coefficient of the order of several hundred μV K^{-1} in magnitude. A bandgap near the Fermi level of the order of 0.1–0.2 eV was measured for these phases [1, 2, 4]. Recent interest in the MNiSn and other half-Heusler phases is due to their promising thermoelectric properties [4–10] and interesting electronic and magnetic structure properties [11–14].

As demonstrated in the bandstructure studies of Tobola *et al* [11], transition metal-based half-Heusler alloys have a high propensity for forming bandgaps. The generality of bandgap formation in these phases can be attributed to the low coordination number of the d-band metals

in the MgAgAs structure. The studies have also found the conducting state of these compounds to be determined by the position of the Fermi level E_F with respect to the gap. For phases with a valence electron count (VEC) of 18, E_F is seen to lie at the top of the highest occupied valence band. Such phases are semiconducting. As the VEC is decreased or increased, E_F is seen to fall below the top of the highest occupied valence band or rise above the bottom of the lowest conduction band, which results in a p-type or n-type semimetallic state, respectively. Extensive studies of Ti-based pseudo-ternary alloys have found a connection between the semiconductor–semimetal (SC–SM) crossover and the onset of a magnetic moment [15, 16]. The connection is explained in the light of the itinerant-electron (itinerant-hole) magnetism picture [11]. Meanwhile, the SC–SM crossover has also been utilized as a working criterion for achieving good thermoelectric properties in the MNiSn class of half-Heusler phases [5, 7, 17].

For the undoped MNiSn phases, SC-like resistivity (ρ) at high T and 'saturation' of ρ at low T have been noted common trends [5, 7, 16–18]. Particularly for the (Zr, Hf)NiSn phases, SM behaviour below 100–150 K and metallic behaviour as $T \rightarrow 0$ have been observed, despite the large ρ-values of 1–3 Ω cm [5, 7, 18] measured at low T. The SM behaviour, together with the small thermopower (S) at low T, have been ascribed to band overlapping [5]. Meanwhile, S has been found to attain a large value of -200 to -400 μV K^{-1} at room temperature [5, 7, 18], which has been attributed to the existence of a moderately heavy electron band mass [5]. The values have been found to be in good agreement with bandstructure results [14]. The reduced gap size with respect to the calculated value and apparent closing of the gap that these semiconducting phases exhibit are probably due to imperfect crystallographic order. Early on, site exchange between the atoms in different sublattices was pointed out [1]. In fact, the transport properties have been reported to be strongly dependent on annealing conditions [1, 5, 7, 11, 18]. Bandstructure studies have shown a reduction in the gap size due to disorder that occurs between the M and Sn metals [13] and also between the two transition metals [19].

The electronic properties found for half-Heusler phases are rather unusual for a metal-based alloy. Further studies of these phases and the semiconductor–semimetal crossover may reveal other interesting properties which may in turn lead to a better understanding of the bandgap structure. Considering the gap reduction reported, one may extend the investigation to semiconducting phases that possess a wider bandgap. We have investigated the electronic transport properties of TiCoSb which has been predicted to be a semiconducting phase with a gap of $\sim$0.95 eV, much wider than that found for the MNiSn phases [11]. We have studied the dependence of properties on the stoichiometry of TiCoSb. High resistivity values in excess of 1000 Ω cm and negative thermopower larger than 400 μV K^{-1} in magnitude, previously not reported for metal-based systems, have been measured. Both n-type and p-type effects have been observed in the doped phases. Unexpectedly, several dopants have been found to enhance the semiconducting behaviour of the host phases.

2. Experimental procedure

Ingots with nominal alloy compositions were prepared by arc melting appropriate quantities of high-purity elements together under an argon atmosphere. The overall purity of the starting materials was 99.996+%. In view of the moderate vaporization of the ingots that occurred during arc melting, most probably due to the higher vapour pressure of Sb, several undoped and doped phases were made using slightly excessive amounts of Sb. The host phases made were TiCoSb, TiCoSb$_{1.02}$, TiCoSb$_{1.05}$, and TiCoSb$_{1.1}$. Chemical analysis using atomic absorption spectroscopy was performed to determine the final compositions of ingots made at the three nominal compositions. Further improvements of the ingots' chemical homogeneity were also attempted by melting pressed pellets of thoroughly mixed elemental powders. However, the

two types of sample were found to exhibit almost identical properties. Two-step annealing was carried out in an evacuated and sealed quartz tube with the sample wrapped in a tantalum foil. The first-stage annealing, carried out at 850 °C for 15 hours, was to homogenize the materials. The second-stage annealing, carried out at 750 °C for 10 days, was to promote the ordering of the crystal structure.

The phase (MgAgAs) purity of the alloys was assessed via x-ray diffraction. The diffraction patterns obtained indicate essentially single-phase samples. A typical pattern for $(Ti_{0.99}V_{0.01})CoSb$ is shown in figure 1. However, investigation of the degree of crystallographic order has not been carried out, and is certainly beyond the scope of the present study. Rectangular pieces, of approximate dimensions $\sim 1.5 \times 2 \times 6$ mm^3, were cut for transport measurements. DC resistivity was measured from 4.2 to 295 K by the four-probe method [18]. Thermopower was measured by the standard differential technique. Copper–constantan thermocouples were used to measure the hot- and cold-end temperatures. The copper leads of the thermocouples were used to measure the thermo-emf. High-temperature resistivity measurements on undoped and vanadium-doped TiCoSb phases were performed following the method described earlier [20].

3. Results and discussion

Chemical analysis has determined the compositions of nominally TiCoSb, $TiCoSb_{1.05}$, and $TiCoSb_{1.1}$ annealed ingots to be $TiCo_{1.01}Sb$, $TiCo_{0.99}Sb$, and $TiCoSb_{1.02}$. Thus, the final

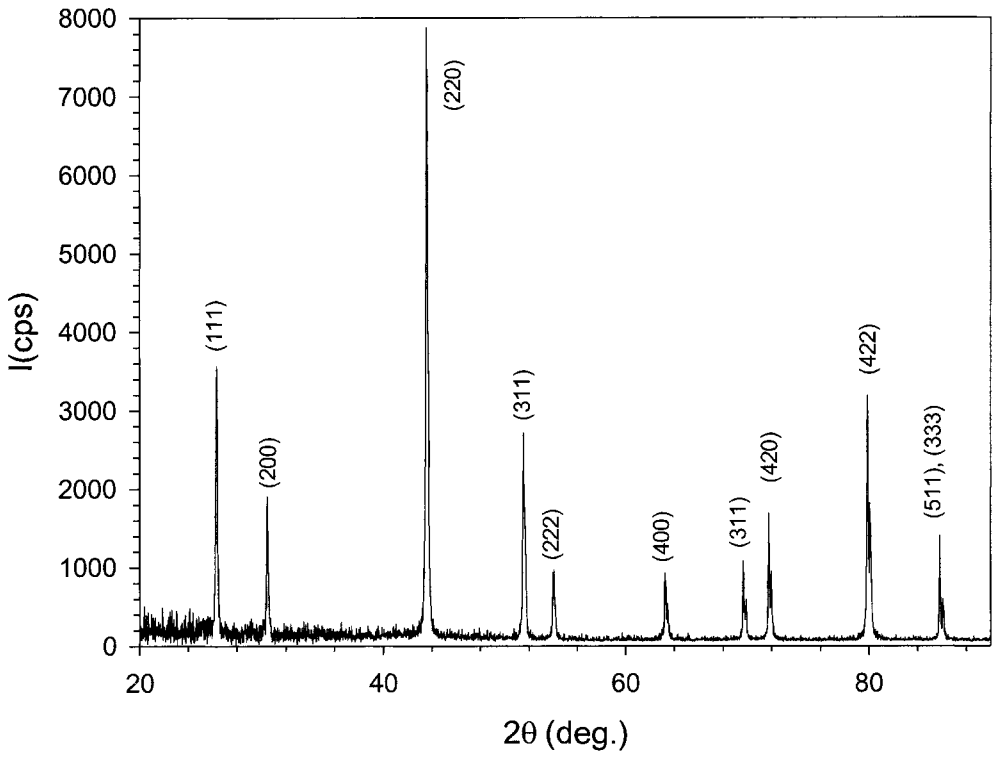

Figure 1. The x-ray diffraction pattern (Cu Kα) for the $(Ti_{0.99}V_{0.01})CoSb$ half-Heusler phase.

compositions are close to the nominal compositions and are quite systematic in TiCo/Sb ratio, despite the moderate vaporization observed during arc melting. Resistivity measurements obtained on the undoped samples of the three compositions and on doped samples based on the three host compositions have been found to be highly reproducible. These findings are attributed to the consistent sample preparation procedure being used. However, it should be pointed out that the standard x-ray diffraction performed is capable neither of detecting very minute volume fractions of impurity phases nor of accessing crystallographic order, beyond the single-phase nature of the well-annealed samples reported.

3.1. Strong dependence of electrical resistivity on ingot sample composition

Resistivity $\rho(T)$ plots for the three host phases are shown in figure 2. Samples obtained after the stage-1 (850 °C/15 h) and stage-2 (stage 1 plus 750 °C/10 days) annealings are presented. In the case of TiCoSb, the $\rho(T)$ curves are reminiscent of a transition from SC to SM states that occurs near 200 K, similar to that reported by another group [16]. However, $TiCoSb_{1.05}$ and $TiCoSb_{1.1}$ exhibit very different $\rho(T)$ behaviour, with high ρ(RT) $\sim$ 1 and 0.6 Ω cm and ρ(4.2 K) $\sim$ 25 and 0.6 Ω cm for the two stage-2 samples, respectively. For the two stage-1 samples, the $\rho(T)$ show rapid upturns at low T, with ρ(4.2 K) reaching as high as ∼100–1600 Ω cm. Earlier, $\rho \sim$ 1–10 Ω cm was reported for another half-Heusler alloy, NbIrSn [21]. Such high ρ-values are unprecedented for a metal-based alloy. In comparison, the dependence of ρ on the stoichiometry is seen to be significantly weaker for other half-Heusler phases [7, 10]. Except for the stage-1 $TiCoSb_{1.05}$, and $TiCoSb_{1.1}$ phases, the $\rho(T)$ trend does not indicate carrier localization, despite the large ρ. With ρ plotted on a log scale,

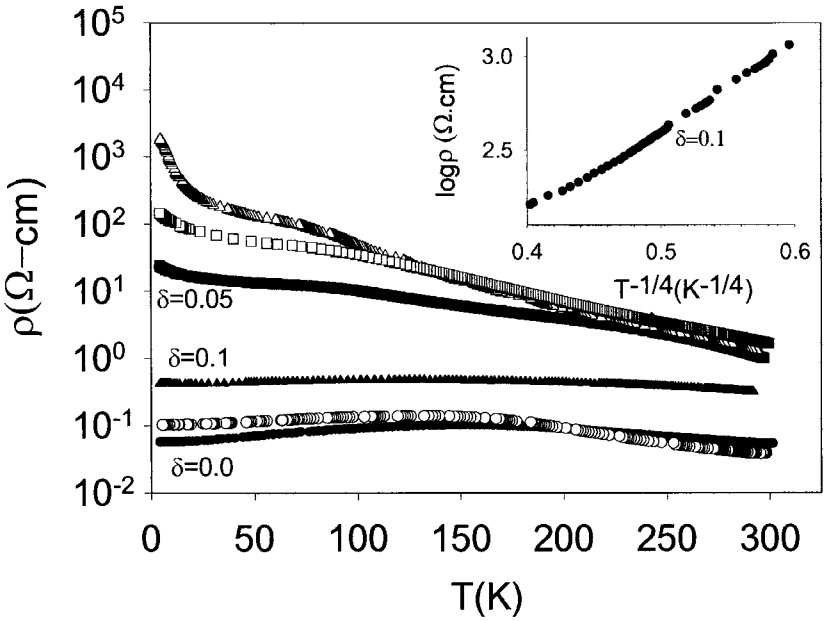

Figure 2. ρ versus T plots for $TiCoSb_{1+\delta}$, where $\delta = 0$, 0.05, and 0.1. The labelled plots (closed symbols) are for stage-2 samples (annealed at 850 °C/15 h + 750 °C/10 days). The unlabelled plots (open symbols) are for stage-1 samples (annealed at 850 °C/15 h). Top to bottom, for the stage-1 samples: $\delta = 0.1$, 0.05, and 0, respectively. Inset: a ρ versus $T^{-1/4}$ plot for a stage-1 $\delta = 0.1$ sample. Results shown in the following figures are all from the stage-2 samples.

the two stage-1 off-stoichiometry phases still show significant upturns at low T. In particular, since the stage-1 $TiCoSb_{1.1}$ sample exhibits a more localized transport behaviour, the data are analysed on the basis of variable-range hopping (VRH). As shown in the inset to figure 2, ρ appears to be proportional to $\exp(T_0/T)^{1/4}$ for 28 K $> T >$ 8 K, where $T_0 \sim 10^4$ K. However, ρ is noted to rise more slowly than that predicted on the basis of VRH below 8 K. Both the localization trend and the deviation from VRH may be attributed to structural disorder in the short-annealed phases.

In view of the actual host compositions obtained, additional stage-2 ingots with composition $TiCoSb_{1.02}$ have also been studied. $\rho(T)$ is found to lie in between those of TiCoSb and $TiCoSb_{1.05}$. Additionally, measurements have been repeated using samples obtained from different ingots of TiCoSb, $TiCoSb_{1.05}$, and $TiCoSb_{1.1}$. The overall composition-dependent $\rho(T)$ trend is found to be reproducible.

3.2. Resistivities of the doped phases

3.2.1. Effects of n-type and p-type dopants. A sampling investigation of doping effects on the unusual resistivities reported in section 3.1 has been performed. The n-type dopants include V, Nb, Ta, and Mn (at Ti sites), Ni and Pt (at Co sites), and Te (at Sb sites). The p-type dopants include Fe (at Co sites), and In and Sn (at Sb sites). Without detailed structural studies, the assignments of doping sites have been mainly based on the known formability of half-Heusler phases [22]. Meanwhile, the very low and near-zero solubilities of the group IIIA elements in Ti have prevented us from performing p-type doping at the Ti site. Previous studies of thermoelectric properties of MNiSn phases have utilized several of the above dopants [5, 7]. Earlier, TiCoSb doped with Sn was also studied with regard to the semiconductor–semimetal and magnetic crossovers [11]. Except for V, our investigation has focused on low doping concentration. In order to evaluate the intrinsic effects due to doping, the study has centred on well-annealed stage-2 samples that are presumed to possess good structural order.

Doping experiments have been repeated using the $TiCoSb_{1.05}$ host. Again, stage-2 samples are studied. Despite the large variation in $\rho(T)$ for the stage-2 host phases (figure 2), the doping trends for the two hosts are found to be essentially similar. That is, for a given dopant, both the range and magnitude of ρ are similar for the doped phases of the two hosts. These findings indicate that the measured doping effects are intrinsic. Apparently, the doping effects are insensitive to any small off-stoichiometry in the host composition, at least for the range of dopant concentrations investigated. This can be understood by noting that even at the lowest doping level ($\sim$0.05% site substitution) studied by us, the density of dopant states ($\geqslant 10^{19}$ cm^{-3}) in the host phases is still significantly larger than the density of carriers in the undoped hosts ($\sim 10^{18}$ cm^{-3} from preliminary Hall effect measurements). Resistivity results on n-doped and p-doped phases are shown in figures 3(a), 3(b), 3(c) and figure 4, respectively. Semimetallic behaviour near room temperature is seen only in the Nb-, Ta-, Pt-, and Te-doped phases. Other dopants either enhance the resistivity (V, Mn, Sn) or are ineffective in reducing the resistivity (Fe, Ni, In). Values of ρ(4.2 K), ρ(300 K), and S(300 K) for both undoped and doped phases are listed in table 1. The effects on Seebeck coefficients are evident in those phases doped with p-type dopants (figure 5 and table 1). The observation of positive S-values reaching $\sim$100 μV K^{-1} upon doping host phases that exhibit a large and negative S(300 K) is in distinct contrast to that reported for p-doped ZrNiSn and HfNiSn [5, 7]. The latter p-doped phases exhibit either negative or very small positive values of S(300 K) of $\sim$+1 μV K^{-1}.

3.2.2. Unusual doping effects of V and Mn. Quite surprisingly, upon doping TiCoSb with the n-type dopants V and Mn, ρ at low T is found to be enhanced instead of reduced. At the

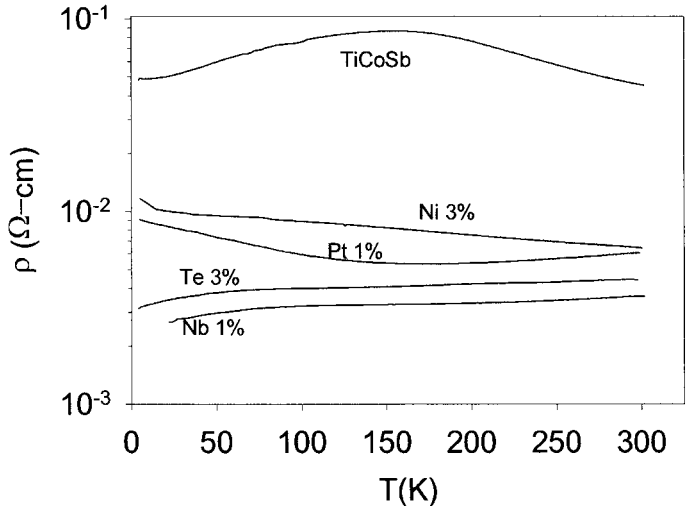

(a)

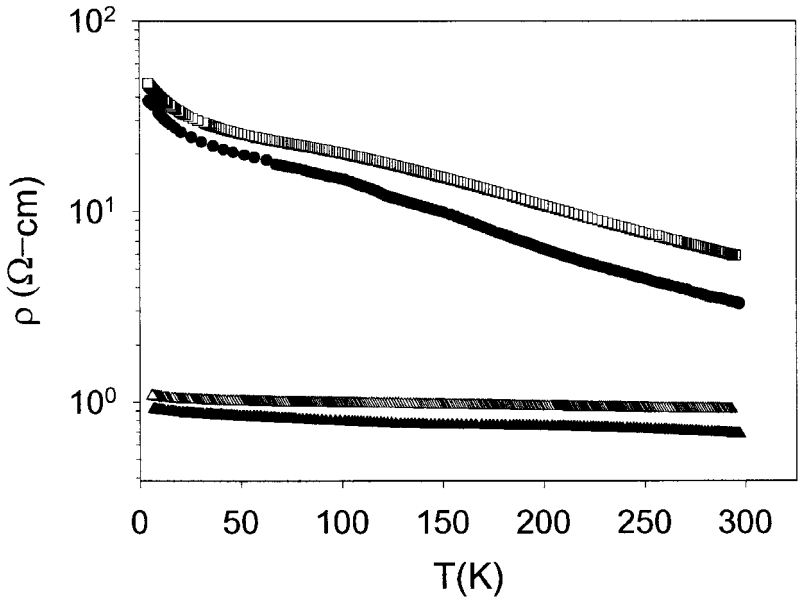

(b)

Figure 3. (a) ρ versus T plots for several n-doped TiCoSb phases. TiCoSb is included for comparison. (b) ρ versus T plots for Mn-doped $TiCoSb_{1+\delta}$ phases (compare figure 2). Top to bottom (refer to the values at 300 K): 0.5% Mn, $\delta = 0.05$; 0.5% Mn, $\delta = 0$; 1% Mn, $\delta = 0.05$; 1% Mn, $\delta = 0$. (c) ρ versus T plots for $(Ti_{1-x}V_x)CoSb$ phases. Top to bottom: $x = 0.005$, 0.01, 0.015, 0.0. Inset: V-doped $TiCoSb_{1.05}$ (upper) and TiCoSb (lower) with $x = 0.005$.

low doping level of $x \leqslant 0.01$, the Mn-doped and V-doped phases exhibit high resistivities $\rho(4.2\ \text{K}) \sim 10$–$50\ \Omega$ cm and $\sim$10–30 Ω cm, respectively. Such enhancement in ρ upon doping has not been seen for other half-Heusler phases. In view of these unusual results, several $\rho(T)$ plots, for the doped phases based on TiCoSb and $TiCoSb_{1.05}$, are displayed in figures 3(b) and 3(c). For each dopant, the similarity in $\rho(T)$ for the two doped hosts illustrates

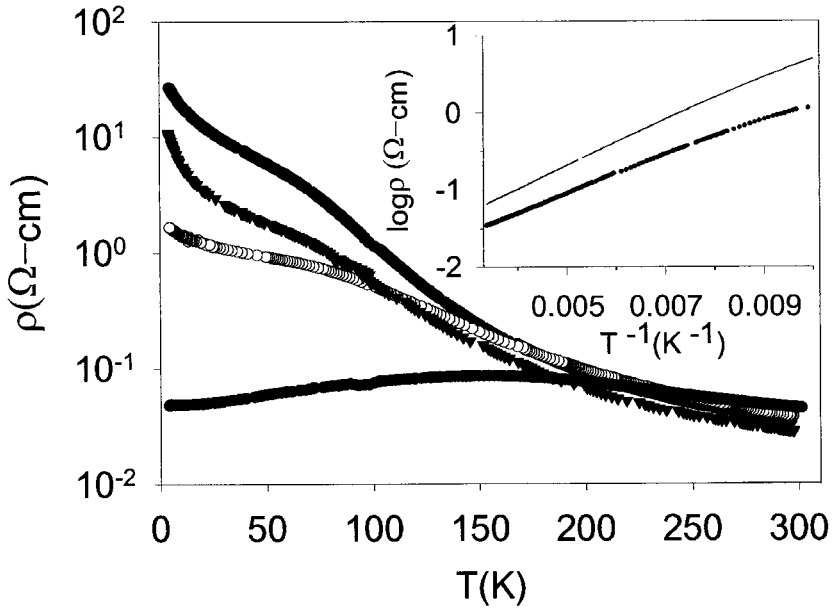

(c)

Figure 3. (Continued)

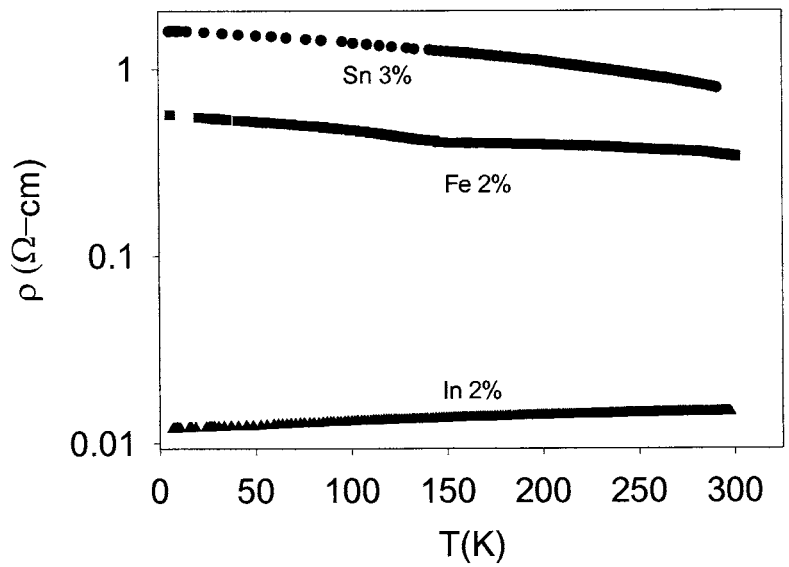

Figure 4. ρ versus T plots for several p-doped TiCoSb phases.

further the intrinsic doping effects noted in section 3.2.1.

To further study the anomalous behaviour observed for the V-doped phases, we first turn to the $\rho(T)$ plots shown in figure 3(c) for $(Ti_{1-x}V_x)CoSb$ at low V content. Plotted on the $\log_{10}$ scale, $\rho(T)$ for the $x = 0.005$ and 0.01 samples displays shoulder-like features between 50 K and 100 K. Although the upturn at low T seems to suggest carrier localization, it is found

Table 1. Resistivity and Seebeck coefficients of TiCoSb host phases (upper data group), n-doped phases (middle data group), and p-doped phases (lower data group) after stage-2 annealing. The tabulated values are obtained by averaging the measurements on at least two samples of a given phase. For the high-ρ $TiCoSb_{1.05}$ and $TiCoSb_{1.1}$ phases and Mn-, Fe-, and Sn-doped phases, the ρ-values can vary by as much as 30% among the samples. Other doped phases show smaller ρ-variation of about 10–20%. Similar or even larger differences in the transport properties of a given alloy system prepared by different groups have also been reported for the MNiSn phases [5, 7, 18].

Alloy phases	ρ(4.2 K) (Ω cm)	ρ(300 K) (Ω cm)	S(300 K) (μV K^{-1})
TiCoSb	5×10^{-2}	4.5×10^{-2}	−265
$TiCoSb_{1.05}$	25	1.2	−500
$TiCoSb_{1.1}$	0.6	0.6	−440
$Ti(Co_{0.99}Ni_{0.01})Sb$	4.7×10^{-2}	1.4×10^{-2}	−250
$Ti(Co_{0.97}Ni_{0.03})Sb$	1.1×10^{-2}	5×10^{-3}	−170
$Ti(Co_{0.9}Ni_{0.1})Sb$	1.5×10^{-3}	1.9×10^{-3}	−75
$Ti(Co_{0.995}Pt_{0.005})Sb$	1.2×10^{-2}	1.1×10^{-2}	−254
$Ti(Co_{0.99}Pt_{0.01})Sb$	9×10^{-3}	5.9×10^{-3}	−260
$(Ti_{0.995}Mn_{0.005})CoSb$	50	5.9	−220
$(Ti_{0.99}Mn_{0.01})CoSb$	7	1.0	−230
$(Ti_{1-x}V_x)CoSb$	*	*	*
$(Ti_{0.99}Nb_{0.01})CoSb$	2.5×10^{-3}	3.7×10^{-3}	−273
$(Ti_{0.98}Nb_{0.02})CoSb$	1.7×10^{-3}	2.9×10^{-3}	−214
$(Ti_{0.97}Nb_{0.03})CoSb$	1.3×10^{-3}	2.3×10^{-3}	−190
$(Ti_{0.99}Ta_{0.01})CoSb$	7×10^{-3}	7.6×10^{-3}	−230
$TiCo(Sb_{0.97}Te_{0.03})$	3.1×10^{-3}	4.5×10^{-3}	−190
$Ti(Fe_{0.02}Co_{0.98})Sb$	0.52	0.34	+ 15
$TiCo(In_{0.02}Sb_{0.98})$	1.2×10^{-2}	1.4×10^{-2}	−13
$TiCo(Sn_{0.01}Sb_{0.99})$	18	2.2	+ 100
$TiCo(Sn_{0.03}Sb_{0.97})$	1.7	0.8	+ 85
$TiCo(Sn_{0.1}Sb_{0.9})$	1.7×10^{-3}	3.8×10^{-3}	−57

* See figures 3(c), 6, 7(a), 7(b).

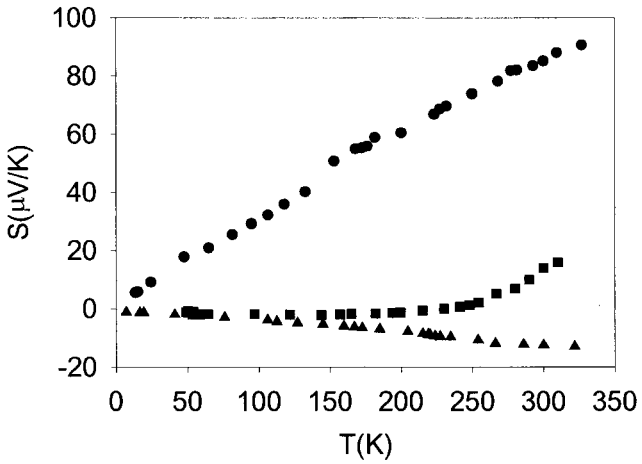

Figure 5. Thermopower versus temperature plots for the p-doped phases shown in figure 4. Top to bottom: 3% Sn, 2% Fe, and 2% In.

that $\rho(T)$ shows neither activated nor hopping conduction behaviour. On the other hand, $\rho(T)$ at $T > 100$ K shows activation conduction behaviour. The latter is illustrated by plotting ln ρ versus $1/T$ for two $x = 0.005$ phases in the inset to figure 3(c). The plots yield an activation energy of ∼0.05 eV above 100 K. The $x = 0.01$ phases also exhibit the same activation energy. On the other hand, activated conduction is absent in all other stage-2 phases that exhibit high ρ-values (figures 2, 3(b), 4).

Semiconductor–semimetal crossover has been investigated in the (Ti, V)CoSb solid solution. With increasing V content, the signature of activated conduction at $T > 100$ K is found to diminish gradually. As can be seen in figure 6, the SC–SM crossover occurs between $x = 0.15$ and 0.2.

3.3. Thermopowers of undoped and doped phases

Very large and negative values of S(300 K) of ∼−400 to −500 μV K^{-1} have been measured for the stage-2 host phases that exhibit high ρ-values (=1 Ω cm). In view of the convergence in the resistivity of the doped hosts noted above, thermopower measurements have been carried out primarily on the doped TiCoSb stage-2 phases (table 1). As a precaution, we have verified that the values of S(300 K) for the various doped hosts do indeed converge for the V, Nb, and Mn dopants. With regard to SC–SM crossover, the thermopower behaviour of $(Ti_{1-x}V_x)$CoSb $(1 \geqslant x \geqslant 0)$ solid solution has been measured, and the results are shown in figure 7. Several features are noted. For the $x = 0.005$–0.015 phases, $S(T)$ exhibits either near-zero or small negative values below ∼60 K but large values from −350 to −420 μV K^{-1} above ∼200 K (figure 7(a)). Similar low-T behaviour of $S(T)$ is also seen in the $TiCoSb_{1.05}$ and $TiCoSb_{1.1}$ phases. Earlier, such low-T thermopower behaviour was ascribed to band overlapping inside the gap [5, 18]. In TiCoSb, band overlapping is also evident from the fact that while the thermopower is negative, preliminary measurements indicate that the Hall coefficient R_H is

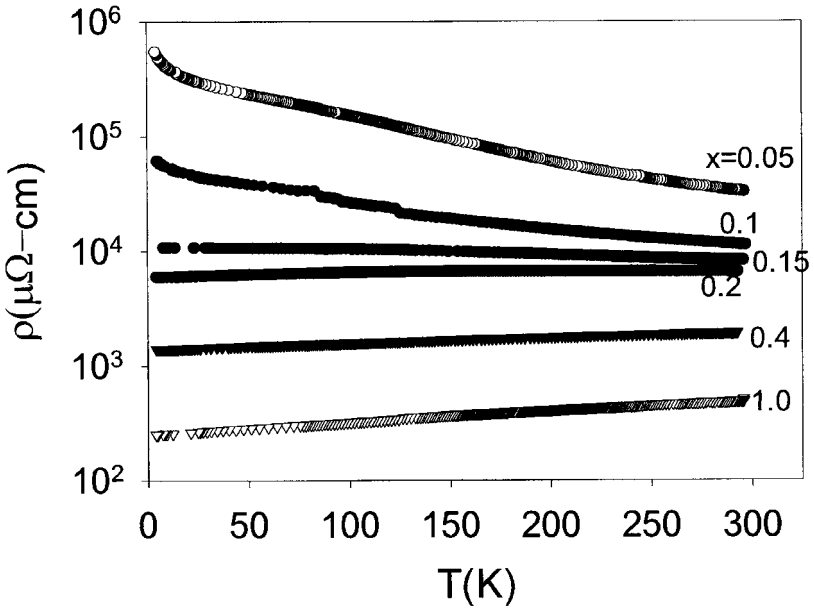

Figure 6. ρ versus T plots for $(Ti_{1-x}V_x)$CoSb spanning both semiconducting and semimetallic regions.

positive at low T. The magnitude of S/T at low T increases with the V dopant content (figure 7(b)). The enhanced n-type transport behaviour underscores the increasing role of the donor electrons.

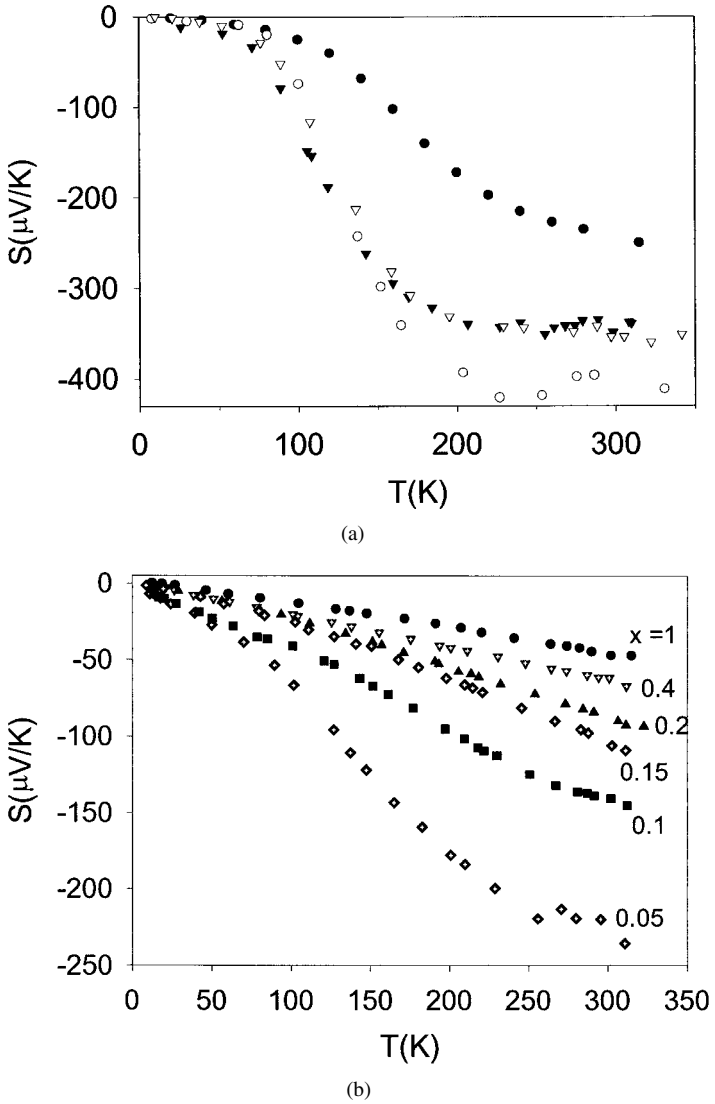

Figure 7. (a) Thermopower versus temperature plots for the lightly doped phases of figure 6. Top to bottom (refer to the values at 300 K): $x = 0$, 0.015, 0.01, and 0.005. (b) Thermopower versus temperature plots for the $x \geqslant 0.05$ phases of figure 6.

3.4. Bandgap features

3.4.1. Effective band mass. Large thermopower values at high T for n-type MNiSn have been attributed to the moderately heavy electron band mass ($m^* \sim 2$–$5\ m$, where m is the free-electron mass) of the conduction band that lies above the gap [5]. m^* has been obtained by solving the one-band equations for the Seebeck coefficient and Hall number over

a wide temperature range. In view of the large thermopower measured in the TiCoSb phases, comparable effective-mass values are expected. We have estimated m^* for the doped phases that exhibit semimetallic resistivity behaviour, such as those seen in alloys doped with more than 10% V and alloys doped with lower concentrations of Nb, Ta, and Te (compare figures 3(a) and 6, table 1). Our estimates are made by using the expression for diffusive thermopower of n-type semimetals described by the 'metallic' formula $S = -(\pi^2 k_B^2 T/3e)\{\mathrm{d}\ln\sigma/\mathrm{d}E\}$ at $E = E_F$ (the Fermi energy), where σ is the electrical conductivity [23], and E_F is measured from the bottom of the conduction band. Furthermore, σ is proportional to $A_F l$, where A_F is the area of the Fermi surface and l is the electronic mean free path. In the parabolic band model, A_F scales as E_F. Taking the scattering time τ of electrons in an alloy as constant, the mean free path $l \sim v_F\tau$ then varies as $E_F^{1/2}$. From these results, the thermopower can be rewritten as $S = -\pi^2 k_B^2 T/2eE_F$. Within the same band model, E_F is proportional to $n^{2/3}/m^*$, where n is the carrier density. Applying the $S(T)$ expression to the $x = 0.15$, 0.2, and 0.4 V-doped phases shown in figure 7(b) and assuming that each vanadium dopant atom contributes one extra electron to the host, m^* is found to be in the range 2–3 m. Similar m^*-values of ∼3–4 m are obtained for the phases lightly doped with Nb, Ta, and Te. Clearly, the m^*-values of the lightly doped alloys are more representative of the electron band mass of the TiCoSb phase than those obtained for the (Ti, V)CoSb solid solutions.

Starting with the large negative thermopowers of the hosts, the positive thermopowers observed upon doping with p-type Sn, Fe, and In (figure 5) suggest that the effective band mass of holes must also be moderately heavy. Large hole band mass comparable to that of the electron has been found in the bandstructure studies of half-Heusler phases [14].

3.4.2. High-temperature resistivities. The ineffectiveness of V, Mn, and Fe as dopants at the low doping level may be attributed to the fact that these 3d dopants tend to retain their valence electrons upon dissolution in the host phase, as has been observed for other doped half-Heusler alloys [11, 12]. However, the electronic picture is less clear for Sn. Overall, the robust doping features of TiCoSb are apparently consistent with the presence of a gap that is wider, and thus better defined, than those of other half-Heusler phases [11, 16].

With the possibility of a wider gap in mind, measurements have been extended to investigate activated conduction in TiCoSb and $(Ti_{0.995}V_{0.005})$CoSb at high temperatures. Figure 8 shows resistivity (as $\log_{10}\rho$) versus temperature from ∼200 K to 800 K. A distinct minimum in $\rho(T)$ can be seen in the region 500–600 K. Clearly, the minimum persists when the data are plotted as $\log_{10}\rho$ versus $1/T$. For certain types of semiconducting compound, such as those based on $FeSi_2$ [24], the latter plot has led to an S-shaped decaying curve. Such a $\rho(T)$ trend has been discussed in the light of the small polaron conduction model, as outlined in reference [24]. According to the latter model, a linear curve has been obtained by plotting $\ln(\rho/T)$ versus $1/T$, with the slope of the linear curve yielding the sum of the activation energy of the dopant level E_d and activation energy of the polaron E_P. For the data shown in figure 8, however, a nearly linear curve can only be obtained if $\ln(\rho/T^n)$, where $2 > n > 1$ rather than $n = 1$, is plotted versus $1/T$. The plots obtained using $n = 1.5$ are illustrated in the inset to figure 8. It is plausible that the value of n, which determines the temperature dependence of the polaron mobility $\mu_P \sim T^{-n}\exp(-E_P/kT)$, is not universal. The plot yields $E_P + E_d \sim 0.06$ eV for both phases. Thus, the activation energy obtained at high temperatures is comparable to that obtained below room temperature (section 3.2.2).

Although the presence of a $\rho(T)$ minimum has prevented us from determining the intrinsic gap, the following remarks can still be made. The resistivity remains high (∼4×10^4 $\mu\Omega$ cm) at 800 K, which is indicative of a larger gap than previously reported [1, 4]. Incidentally,

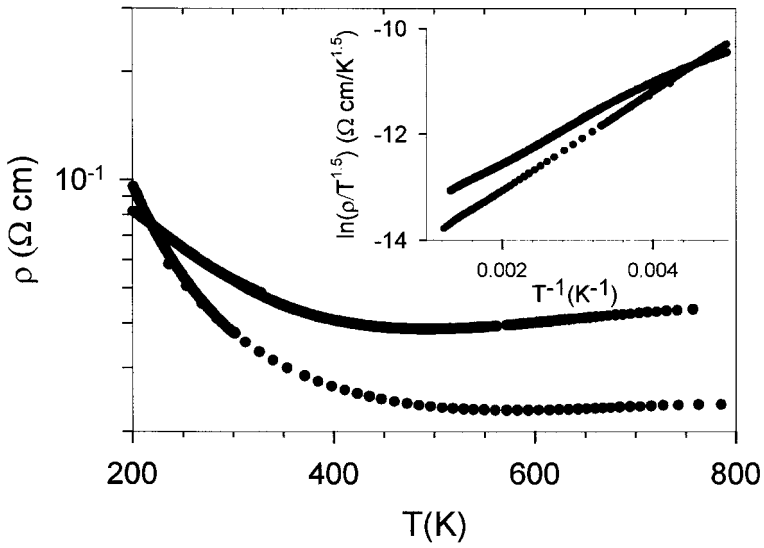

Figure 8. ρ versus T plots for TiCoSb (upper) and ($Ti_{0.995}V_{0.005}$)CoSb (lower). ρ is plotted on the $\log_{10}$ scale. Thus, the values of ρ(300 K) for the two phases are $\sim$0.05 $\mu\Omega$ cm and 0.035 $\mu\Omega$ cm, respectively. Inset: $\ln(\rho/T^{1.5})$ is plotted against $1/T$ for the two phases.

$FeSi_2$ exhibits a comparable resistivity at $\sim$800 K [24]. In fact, $FeSi_2$ has been known to have a semiconducting gap of $\sim$1 eV. Further understanding of charge transport in the present metal-based alloys will require systematic measurements of resistivity, thermopower, and the Hall coefficient at high temperatures.

4. Conclusions

Arc-melted half-Heusler TiCoSb phases with compositions approaching ever closer to that of 1–1–1 stoichiometry have been made by using a slightly excess amount of Sb in the starting material. The undoped phases that are not deficient in Sb have been found to have significantly larger resistivity and thermopower than those reported for the nominally 1–1–1 ingots. The unprecedented high resistivity and high Seebeck coefficient, as well as the robust n-type and p-type doping characteristics, are unusual findings for a metal-based compound. The high resistivity has been found to persist in measurements reaching 800 K. These results have revealed important differences between the semiconducting properties of TiCoSb and those of other metal-based half-Heusler phases studied to date. Many of the latter phases have been shown to possess a bandgap of $\sim$0.1–0.2 eV. Overall, the findings are consistent with the existence of a wider gap in TiCoSb, as predicted by a bandstructure calculation. Meanwhile, the presence of an additional conduction mechanism at high temperatures, possibly due to light polarons, has prevented us from determining the size of the gap. Despite the difficulty in attaining perfect crystallographic order in the half-Heusler phases and therefore the possibility that the intrinsic properties of TiCoSb have not been fully uncovered, the properties observed have been found to resemble those of nonmetal-based semiconductors. Thus, these phases can already be utilized as model systems for more detailed studies of the bandgap and electronic state in metal-based compounds. Future studies will include optical reflectivity and magnetoconductivity measurements.

Acknowledgments

The work at the University of Virginia is supported by NSF Grant No DMR 97-00584. The work at Clemson University is supported by DARPA/ARO No DAAG55-97-1-0-267, ONR No N00014-98-1-0271, and ONR No N00014-98-1-0444.

References

[1] Aliev F G, Brandt N B, Moschalkov V V, Kozyrkov V V, Skolozdra R V and Belogorokhov A I 1989 *Z. Phys.* B **75** 167
[2] Aliev F G, Kozyrkov V V, Moschalkov V V, Skolozdra R V and Durczewski K 1990 *Z. Phys.* B **80** 353
[3] Jeischko W 1970 *Metall. Trans.* A **1** 3159
[4] Cook B A, Harringa J L, Tan Z S and Jesser W A 1996 *Proc. ICT'96: 15th Int. Conf. on Thermoelectrics* (Catalog No 96TH8169) (Piscataway, NJ: IEEE) p 122
[5] Uher C, Yang J, Hu S, Morelli D T and Meisner G P 1999 *Phys. Rev.* B **59** 8615
[6] Hohl H, Ramirez A R, Kaefer W, Fess K, Thurner Ch, Kloc Ch and Bucher E 1997 *Thermoelectric Materials—New Directions and Approaches (MRS Symp. Proc. vol 478)* ed T M Tritt, M Kanatzidis, H B Lyon Jr and G D Mahan (Warrendale, PA: Materials Research Society) p 109
[7] Hohl H, Ramirez A P, Goldmann C, Ernst G, Woelfing B and Bucher E 1999 *J. Phys.: Condens. Matter* **11** 1697
[8] Browning V M, Poon S J, Tritt T M, Pope A L, Bhattacharya S, Volkov P, Song J G, Ponnambalam V and Ehrlich A C 1999 *Thermoelectric Materials 1998—the Next Generation Materials for Small-Scale Refrigeration and Power Generation Applications (MRS Symp. Proc. vol 545)* ed T M Tritt, M Kanatzidis, H B Lyon Jr and G D Mahan (Warrendale, PA: Materials Research Society) p 403
[9] Sportouch S, Larson P, Bastea M, Brazis P, Ireland J, Kannenwurf C R, Mahanti S D, Uher C and Kanatzidis M G 1999 *Thermoelectric Materials 1998—the Next Generation Materials for Small-Scale Refrigeration and Power Generation Applications (MRS Symp. Proc. vol 545)* ed T M Tritt, M Kanatzidis, H B Lyon Jr and G D Mahan (Warrendale, PA: Materials Research Society) p 421
[10] Mastronardi K, Young D, Wang C C, Khalifah P, Cava R J and Ramirez A P 1999 *Appl. Phys. Lett.* **74** 1415
[11] Tobola J, Pierre J, Kaprzyk S, Skolozdra R V and Kouacou M A 1998 *J. Phys.: Condens. Matter* **10** 1013
[12] Kaczmarska K, Pierre J, Tobola J and Skolozdra R V 1999 *Phys. Rev.* B **60** 373
[13] Ogut S and Rabe K M 1995 *Phys. Rev.* B **51** 10 443
[14] Mahanti S D, Larson P, Chung D Y, Sportouch S and Kanatzidis M G 1999 *Thermoelectric Materials 1998—the Next Generation Materials for Small-Scale Refrigeration and Power Generation Applications (MRS Symp. Proc. vol 545)* ed T M Tritt, M Kanatzidis, H B Lyon Jr and G D Mahan (Warrendale, PA: Materials Research Society) p 23
[15] Pierre J, Skolozdra R V, Gorelenko Yu K and Kouacou M 1994 *J. Magn. Magn. Mater.* **134** 95
[16] Pierre J, Skolozdra R V, Tobola J, Kaprzyk S, Hordequin C, Kouacou M A, Karla I, Currat R and Lelievre-Berna E 1997 *J. Alloys Compounds* **262–263** 101
[17] Poon S J, Tritt T M, Xia Y, Bhattacharya S, Ponnambalam V, Pope A L, Littleton R T and Browning V M 1999 *Proc. ICT'99: 18th Int. Conf. on Thermoelectrics* (IEEE Catalog No 99TH8407) (Piscataway, NJ: IEEE) p 45
[18] Ponnambalam V, Pope A L, Bhattacharya S, Xia Y, Poon S J and Tritt T M 1999 *Proc. ICT'99: 18th Int. Conf. on Thermoelectrics* (IEEE Catalog No 99TH8407) (Piscataway, NJ: IEEE) p 340
[19] Orgassa D, Fujiwara H, Schulthess T C and Butler W H 1999 *Phys. Rev.* B **60** 13 237
[20] Littleton R T, Jeffries J, Kaeser M A, Long M and Tritt T M 1999 *Thermoelectric Materials 1998—the Next Generation Materials for Small-Scale Refrigeration and Power Generation Applications (MRS Symp. Proc. vol 545)* ed T M Tritt, M Kanatzidis, H B Lyon Jr and G D Mahan (Warrendale, PA: Materials Research Society) p 137
[21] Hohl H, Ramirez A P, Goldmann C, Ernst G, Woelfing B and Bucher E 1998 *J. Phys.: Condens. Matter* **10** 7843
[22] Villars P and Calvert L D 1991 *Pearson's Handbook of Crystallographic Data for Intermetallic Phases* 2nd edn, vols 1–4 (Metals Park, OH: ASM International)
[23] Mott N F and Davis E A 1971 *Electronic Processes in Non-Crystalline Materials* (Oxford: Clarendon)
[24] Kojima T 1989 *Phys. Status Solidi* a **111** 233